Solar Wind Control of Magnetosheath Jet Formation and Propagation to the Magnetopause

Adrian T. LaMoury[1], Heli Hietala[1], Ferdinand Plaschke[2], Laura Vuorinen[3], and Jonathan P. Eastwood[1]

[1]The Blackett Laboratory, Imperial College London, London, UK
[2]Space Research Institute, Austrian Academy of Sciences, Graz, Austria
[3]Department of Physics and Astronomy, University of Turku, Turku, Finland

Key Points:

- THEMIS and OMNI data from 2008–2018 are used to constrain conditions for jet formation and propagation to the magnetopause
- Jets reach the magnetopause 17x more often during low IMF cone angles ($< 33°$) and 8x more often during high solar wind speeds (> 539 km/s)
- Low IMF magnitude, high Alfvén Mach no., and low density double expected magnetopause impacts, dynamic pressure and β have no net effect

Corresponding author: Adrian LaMoury, adrian.lamoury15@imperial.ac.uk

Abstract

Magnetosheath jets are localized high-dynamic pressure pulses originating at Earth's bow shock and propagating earthward through the magnetosheath. Jets can influence magnetospheric dynamics upon impacting the magnetopause; however many jets dissipate before reaching it. In this study we present a database of 13,096 jets observed by the Time History of Events and Macroscale Interactions during Substorms (THEMIS) spacecraft from 2008–2018, spanning a solar cycle. Each jet is associated with upstream solar wind conditions from OMNI. We statistically examine how solar wind conditions control the likelihood of jets forming at the shock, and the conditions favorable for jets to propagate through the magnetosheath and reach the magnetopause. We see that, for each solar wind quantity, these two effects are separate, but when combined, we find that jets are over 17 times more likely to reach and potentially impact the magnetopause when the interplanetary magnetic field (IMF) orientation is at a low cone angle, and approximately 8 times more likely during high speed solar wind. Low IMF magnitude, high Alfvén Mach number, and low density approximately double the number of jets at the magnetopause, while β and dynamic pressure display no net effect. Due to the strong dependence on wind speed, we infer that jet impact rates may be solar cycle dependent as well as vary during solar wind transients. This is an important step towards forecasting the magnetospheric effects of magnetosheath jets, as it allows for predictions of jet impact rates based on measurements of the upstream solar wind.

Plain Language Summary

When the solar wind, a constant flow of plasma from the Sun, meets Earth's magnetic field, a shock wave forms in space. Like a rock in a stream, the plasma is diverted around the obstacle and a dense, turbulent layer — the magnetosheath — forms in front of it. We study instances of fast plasma jets bursting through the shock and traveling towards Earth. However, it appears that only a small proportion of jets hit the edge of our magnetic field — the magnetopause. To forecast their effects, we therefore need to know when jets will make it through. We use a database of 13,096 jets observed by spacecraft in the magnetosheath, alongside measurements of the solar wind, to determine when jets are most likely to hit the magnetopause. We find the highest probability is when the solar wind magnetic field is aligned with its flow direction and when it has a higher speed. We hope that, with this information, we may eventually be able to forecast space weather effects of jets based solely on measurements of the upstream solar wind.

1 Introduction

Magnetosheath jets, also referred to as 'high-speed jets' (HSJs; Plaschke et al., 2013), 'dynamic pressure enhancements' (Archer & Horbury, 2013), or 'plasmoids' (Karlsson et al., 2015) (hereafter referred to simply as 'jets'), are localized high-dynamic pressure pulses observed in the magnetosheath (see Plaschke et al., 2018, and references therein for a comprehensive review). Jets are seen approximately 9 times more often downstream of the quasi-parallel shock, that is, where the angle between the interplanetary magnetic field (IMF) and the local shock normal is less than 45°, than the quasi-perpendicular shock (Archer & Horbury, 2013; Plaschke et al., 2013; Vuorinen et al., 2019). Recently, Raptis et al. (2020) studied the differences between jets found downstream of the quasi-parallel shock versus those downstream of the quasi-perpendicular shock, finding that they display different properties, with quasi-perpendicular jets being generally weaker in terms of velocity, density, and duration. A variety of jet formation processes have been suggested. A prominent theory is that jets originate from the non-uniform processing of solar wind plasma through ripples in the quasi-parallel bow shock surface and propagate earthward (Hietala et al., 2009, 2012). Ripples are generally thought to be the result of foreshock structures, such as short large-amplitude magnetic structures (SLAMS), merg-

ing to form the shock (e.g, Schwartz & Burgess, 1991), hence this mechanism takes place predominantly at the quasi-parallel shock. In addition, there is evidence to suggest that some jets may form from the interaction of SLAMS with bow shock ripples (Karlsson et al., 2015; Palmroth et al., 2018; Raptis et al., 2020). Several other formation mechanisms have been proposed, such as rotational discontinuities in the IMF (e.g, Archer et al., 2012; Dmitriev & Suvorova, 2012).

As they propagate into the magnetosheath, generally at higher velocities than their surroundings, magnetosheath jets can disturb the local plasma environment by driving bow waves and secondary particle accelerating shocks ahead of them (e.g., T. Z. Liu et al., 2020). If jets go on to hit the magnetopause they may produce magnetospheric effects. As their dynamic pressure is enhanced with respect to the surrounding magnetosheath, they can indent and rebound from the magnetopause surface (Amata et al., 2011; Dmitriev & Suvorova, 2015; Shue et al., 2009), launch propagating waves (Archer et al., 2014), or create surface eigenmodes, as was suggested by Plaschke et al. (2009) and recently observed by Archer et al. (2019). In addition, the increased dynamic pressure they present can compress the magnetopause current sheet, stimulating magnetic reconnection. This was observed by Hietala et al. (2018) who reported in situ observations of reconnection triggered by a jet impact. They saw that, despite favorable conditions in terms of magnetic field alignment and β-shear (see, e.g., Swisdak et al., 2010), reconnection was prevented by the magnetopause layer being too thick. However, following a jet impact, this layer was sufficiently compressed that reconnection onset was observed. In another case study, Nykyri et al. (2019) inferred that a substorm was triggered by a jet bringing southward B_Z to the magnetopause during a period of northward IMF. A number of other potential interactions have been studied. For example, Dmitriev and Suvorova (2015) suggested that jets may stimulate impulsive penetration of magnetosheath plasma into the magnetosphere, while Wang et al. (2018) observed that jet impacts are linked to auroral brightenings. In addition, dayside 'throat' auroras have been linked to magnetopause indentations, potentially arising from jet impacts during times of quasi-radial IMF (Han et al., 2018).

The aforementioned effects involve the interaction of jets with the magnetopause. Jets are believed to impinge upon the magnetopause very often: Large scale magnetosheath jets, with a cross-sectional diameter of $2\,\mathrm{R_E}$ or greater, have been estimated to impact the magnetopause several times per hour, with smaller jets potentially impacting hundreds or thousands of times per hour (Plaschke et al., 2016; Plaschke, Hietala, & Vörös, 2020). Therefore, in order to eventually forecast magnetospheric effects arising from jets, we must first establish when jets are most likely to reach the magnetopause. In their statistical study, Plaschke et al. (2013) determined that jets are most commonly observed near and shortly downstream of the bow shock, with the probability of observation falling dramatically close to the magnetopause, suggesting that they are often dissipated, braked, or broken up during propagation. This idea has been supported by simulations such as those by Karimabadi et al. (2014) and Omidi et al. (2016) where jets have been seen to face instabilities and turbulence during their propagation. In addition, a recent study by Palmroth et al. (2021) combined jet observations from the Magnetospheric Multiscale spacecraft (MMS; Burch et al., 2016) with global hybrid-Vlasov simulations to examine how jet properties evolve as they propagate. They found that the jet's density, dynamic pressure, and magnetic field magnitude all fall from the bow shock to the magnetopause, while temperature rises, making near-magnetopause jets more akin to the surrounding plasma.

Despite their potential magnetospheric effects, there has been relatively little work to date on understanding what controls jet propagation, particularly with respect to the upstream solar wind and forecasting. One suggestion was made by Goncharov et al. (2020), by simple comparison of observed jet distances from a model bow shock, that jets propagate deeper into the magnetosheath downstream of the quasi-parallel shock than down-

stream of the quasi-perpendicular shock. In the subsolar region of the magnetosheath this corresponds to low cone angle (the acute angle between the IMF and the Sun-Earth line) solar wind, which is now also a well-established favorable condition for jet formation, with minor dependencies on solar wind speed, density, and IMF stability noted by Plaschke et al. (2013) and Archer and Horbury (2013).

The focus of the present work is, therefore, on determining what upstream solar wind conditions are most favorable for large numbers of jets to reach and impact the magnetopause, with a view to informing future forecasting regimes. We further break this problem down into two components: probability of jet formation at the bow shock, and probability of propagation to the magnetopause. We consider these two processes separately, as it is not immediately obvious whether, for a given solar wind quantity, they would reinforce or counteract each other. When combined, the net effect paints a picture of how different solar wind conditions affect the overall rate of jets reaching the magnetopause. Using a large data set of jets observed over 11 years, with a variety of corresponding upstream solar wind conditions, we statistically determine the most favorable conditions to be those associated with the fast solar wind, with low IMF cone angle and high solar wind speed being the most strongly controlling properties. We see weak dependencies on IMF magnitude, Alfvén Mach number, and density, while plasma β and solar wind dynamic pressure have no net effect.

In the next section we introduce the data set used in this study and describe our analysis techniques. In Section 3 we present the results of our analyses on jet formation and propagation, with their combined significance discussed in Section 4. Finally, in Section 5 we summarize our findings and make suggestions for future work.

2 Data and Methods

2.1 Data Set

In this study we use a database of 13,096 jet observations made by the five Time History of Events and Macroscale Interactions during Substorms spacecraft (THEMIS; Angelopoulos, 2008) from 2008 to 2018 (inclusive). Data are available from Plaschke, Hietala, and Angelopoulos (2020) for 2008–2011, and Plaschke, Hietala, and LaMoury (2020) for 2012–2018. Jets are selected from over 31 million (8,713.5 hours) magnetosheath measurements. The full data set is presented here for the first time, though it should be noted that it contains the 2,859 jets first presented by Plaschke et al. (2013), and was compiled using the same methods. We give some comparative statistics for each data set in Table 1. For a full description of the algorithmic detection we therefore refer the reader to Plaschke et al. (2013), and here we summarize the key points relevant to this work. THEMIS data are interpolated such that all measurements share a common one second cadence. Each measurement in the magnetosheath is then associated with upstream solar wind conditions taken from the OMNI database (King & Papitashvili, 2005), averaged for the preceding five minutes. Initially, intervals where a THEMIS probe was determined to be in the subsolar region are selected. That is, observations made within a 30° cone with Earth at the tip, symmetrical about the Sun-Earth line, and between 7 and 18 R_E radially from the center of Earth. We then ensure that we select only magnetosheath data by requiring that the ion density must exceed twice that of the upstream solar wind and that the energy flux of 1 keV ions is greater than that of 10 keV ions. All these conditions must be satisfied for at least two continuous minutes, therefore excluding partial boundary crossings and foreshock structures that typically have shorter timescales. From these intervals, jets are identified as instances where the maximum X_{GSE}-directed dynamic pressure measured in the magnetosheath exceeds half that of the pristine solar wind. We use this criterion as it is most relevant for forecasting magnetopause impacts. Leading and trailing edges of each jet are defined as the closest points either side of the maximum where dynamic pressure drops below a quarter of the solar wind value. Note,

Table 1. Comparison of key statistics between data sets.

Property	2008–2011	2012–2018	2008–2018
Magnetosheath data (hours)	2,501.1	6,212.4	8,713.5
Magnetosheath data outside model boundaries (hours)	283.5 (11 %)	751.7 (12 %)	1035.3 (12 %)
Number of jets	2,859	10,237	13,096
Number of jets outside model boundaries	202 (7 %)	375 (4 %)	577 (4 %)
Number of jets $F < 0.25$ (near MP)	678	1,256	1,924
Number of jets $F > 0.75$ (near BS)	313	1,426	1,739

Note. Data from 2008–2011 were first introduced by Plaschke et al. (2013), while those from 2012–2018 are presented here for the first time. This study makes use of both data sets combined (last column). Magnetosheath boundaries are given by the empirical models of Shue et al. (1998) and Merka et al. (2005), and F is the fractional distance through this model magnetosheath, as described in the text.

however, that the analysis presented in this study considers only the solar wind conditions associated with the point of maximum dynamic pressure ratio within each jet.

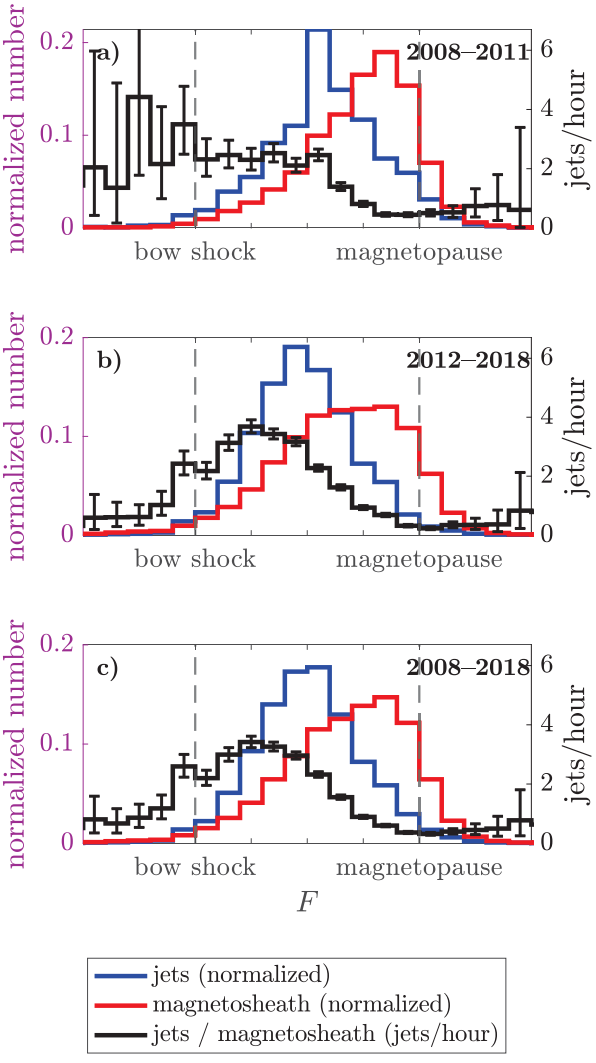
We extend the four-year database of Plaschke et al. (2013), covering only the solar minimum, to a full solar cycle for several reasons. The aim of this study is to make a step towards understanding and forecasting the space weather effects of jets. Naturally, space weather studies are generally concerned with extreme events, with many effects showing some kind of solar cycle dependence. For example, from 2008 to 2011, only 12 % (292 hours) of magnetosheath data corresponded to upstream solar wind speeds of above $500\,\mathrm{km\,s^{-1}}$ with a maximum observed speed of $736\,\mathrm{km\,s^{-1}}$, compared to 23 % (1433 hours) and a maximum of $846\,\mathrm{km\,s^{-1}}$ in the 2012–2018 data set, which contains the solar maximum.

The variable dynamic pressure of the solar wind causes the magnetopause and bow shock positions to fluctuate, altering the thickness of the magnetosheath layer. Therefore, in order to meaningfully compare factors affecting jet propagation through the magnetosheath, we place each observation on a normalized relative distance scale. This is calculated by

$$F = \frac{R - R_{\mathrm{MP}}}{R_{\mathrm{BS}} - R_{\mathrm{MP}}}, \tag{1}$$

where R is the radial distance of the spacecraft from Earth, R_{MP} the radial distance to a model magnetopause, and R_{BS} the radial distance to a model bow shock, such that $F = 1$ at the bow shock and 0 at the magnetopause (Archer & Horbury, 2013). The models used for the magnetopause and bow shock are those by Shue et al. (1998) and Merka et al. (2005) respectively, and solar wind conditions from OMNI are used as model inputs. Note that this treats the magnetosheath as a one-dimensional layer and is suitable for the subsolar region, where our observations were made. The jet detection algorithm would require a different approach at the flanks and at higher latitudes, where the overall magnetosheath flow is faster than in the subsolar region (see also Qu et al., 2021).

Figure 1 shows the distribution of jet observation positions within this one-dimensional model magnetosheath. Figure 1a shows the 2,859 jets presented by Plaschke et al. (2013), Figure 1b shows the new data set containing 10,237 jets measured by THEMIS from 2012 to 2018 (inclusive), while Figure 1c shows these two data sets combined. In each, the red histograms show the location of all measurements made in the magnetosheath. We see these distributions peak at $0.1 < F < 0.2$, indicating that the THEMIS probes spent more time near the magnetopause than near the bow shock. Blue histograms show the observation locations of jets, selected from the magnetosheath intervals. From these we see that most jets were observed near the middle of the magnetosheath, at $F \sim 0.5$.



1.pdf

Figure 1. Distributions of observation locations through model magnetosheath. Jet observations are shown in blue while the whole magnetosheath data set from which they are selected is shown in red. Both are normalized for ease of comparison and therefore correspond to the left y-axis. The black histograms give the probability distributions accounting for orbital effects, expressed in units of jets observed per hour spent in the magnetosheath at that F-range (right hand y-axis). a) THEMIS measurements from 2008–2011, as presented by Plaschke et al. (2013); b) new data set from 2012–2018; c) both data sets combined.

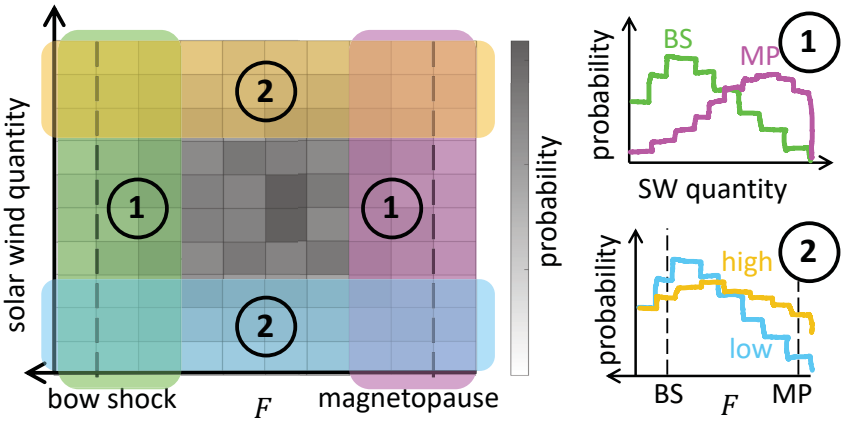
In order to make meaningful statements about jet observation probability, we must account for the non-uniform sampling of the magnetosheath. To do this, we divide each bin of the jet distribution by the corresponding bin of the magnetosheath distribution. This produces the black distribution, which is also scaled to units of jets observed per hour spent in the magnetosheath, per bin. The black histogram is, therefore, a probability distribution for jet observation location in the magnetosheath, free of biases arising from spacecraft orbits as it shows how commonly jets are observed in each location, relative to the amount of time spent there by spacecraft. Error bars are estimated using the Clopper-Pearson method to calculate a 95 % binomial confidence interval, and therefore are larger when there are fewer data in a given bin (e.g., Brown et al., 2001).

Figure 1 therefore implies that jets are most likely to be observed downstream of the bow shock, with the probability of observation dropping towards the magnetopause. This is consistent with the idea that they are formed from the interaction of solar wind with bow shock ripples (Hietala et al., 2009, 2012). As we are concerned with understanding what allows jets to propagate from the bow shock to the magnetopause, we require a sufficient number of jet observations near these boundaries. Herein, we therefore make use of the combined data set as whole, making no distinction between the older and newer data.

There is some amount of uncertainty regarding a jet's exact location with respect to the boundaries. As shown in Table 1, 12 % of time spent in the magnetosheath (red curves in Figure 1) and 4 % of jet observations (blue curves in Figure 1) are determined to be outside of our model boundaries despite the fact that the selection criteria are such that all data are determined to be from the magnetosheath. Note that it is not meaningful to consider regions outside of the boundaries on the black curves of Figure 1, as these do not show raw data. Though commonly used, the empirical models may have limitations. For example, Suvorova et al. (2010) suggested that, under prolonged periods of quasi-radial IMF, the magnetopause position may lie significantly further out than what is predicted by the Shue et al. (1998) model, due to the foreshock being located directly upstream of the Earth and decreasing the pressure in the magnetosheath and on the magnetopause. In addition, Z.-Q. Liu et al. (2015) determined, with the use of MHD models, that the magnetopause location can deviate from the Shue et al. (1998) model when accounting for changing IMF orientations and the Earth's dipole tilt. To account for these uncertainties, we will keep our bin size coarse (one quarter of the model magnetosheath thickness). The models are driven by data from OMNI, which naturally contain some uncertainty as they are algorithmically propagated to the bow shock from measurements at L1. We do not consider this to be a significant issue, however, as any forecasting regime developed from our results would likely encounter the same limitations.

2.2 Investigating Solar Wind Control of Jet Formation and Propagation

To understand what affects the probability of jet formation, we use the database to produce probability distributions showing the likelihood of observing a jet near the bow shock as a function of relevant solar wind parameters. As with Figure 1, we normalize jet distributions by the corresponding distribution for magnetosheath measurements. To account for non-uniform sampling of the parameter space, each bin of jet observations is therefore divided by the corresponding bin of the magnetosheath data set from which jets are selected, under the same conditions. The resulting distribution thus shows how likely a jet is to form under certain solar wind conditions, given that those conditions are observed. Note that a similar analysis was performed by Plaschke et al. (2013). A crucial difference here, however, is that we restrict our analysis to only jets and magnetosheath observations made near the bow shock (those with $F > 0.75$) so



2.pdf

Figure 2. a) Cartoon of the parameter space explored to determine how solar wind conditions affect jet propagation. In method 1 (panel b), normalized probability distributions of solar wind quantities are compared for near-bow shock (green region) and near-magnetopause (magenta) jets. In method 2 (panel c), normalized probability distributions in F are compared for high (orange) and low (cyan) values of each solar wind quantity.

that potential differences in jet propagation probability do not influence conclusions on factors affecting jet formation.

To be geoeffective, jets must interact with the magnetopause. It is therefore important to determine why some jets are able to travel further than others, and, with a particular view to forecasting, what solar wind conditions are favorable for jets propagating through the magnetosheath and reaching the magnetopause. We approach this problem via two analysis techniques, which are illustrated in Figure 2a where we show a cartoon of the parameter space to be explored. Note that, with single spacecraft observations of each jet, we cannot directly observe jets terminating or estimate their eventual propagation depth. The population of jets observed near the bow shock therefore contains jets that later went on to strike the magnetopause, as well as those that dissipated shortly downstream of the shock. We can infer the conditions most favorable for jets to reach the magnetopause, however, by isolating the population of jets observed shortly in front of it. If a jet is observed in the green region of Figure 2a, near the bow shock, we do not know where it will dissipate, however, comparing distributions at different F values, we are able to infer the conditions conducive to jet propagation. If jet propagation depth is dependent on a particular solar wind parameter, we would expect to see a change in the distribution of this parameter corresponding to jet observations at different depths into the magnetosheath (different values of F). Our first method for establishing how the solar wind conditions affect jet propagation is, therefore, to compare the solar wind parameter probability distributions for newly formed jets close to bow shock ($F > 0.75$, the region highlighted in green in Figure 2a), with jets observed reaching the magnetopause ($F < 0.25$, magenta). Differences between the two distributions (Figure 2b) may indicate that the solar wind quantity in question has an influence on the ability of a jet to propagate to the magnetopause.

The second approach (Figure 2c) taken is to compare relative distance (F) distributions (as in Figure 1) filtered by extreme values of each solar wind parameter. These can be interpreted as the orange and cyan regions in Figure 2a. Threshold values are set

at the 85^{th} and 15^{th} percentiles of the magnetosheath distribution for each solar wind parameter, thus corresponding to 'high' and 'low' regimes. As jet occurrence falls from the bow shock to the magnetopause, we expect most distributions to broadly follow this trend. A difference in gradient between the two distributions, however, implies that a solar wind quantity may influence expected jet propagation depth. If a particular solar wind condition is highly favorable for jet survival, we expect its distribution to be flatter. In both methods we use the normalization technique described previously, so that the resulting plots are probability distributions.

3 Results

3.1 Factors Affecting Jet Formation

Figure 3 shows probability distributions for jet formation at the bow shock as a function of each solar wind parameter studied. As mentioned previously, these are comparable with the analyses of Plaschke et al. (2013), except that we restrict to only jets and magnetosheath data recorded near the bow shock ($F > 0.75$; green in Figure 2a) so as to isolate factors affecting jet formation from other effects that may influence the likelihood of jet observation. As in Figure 1, blue histograms represent raw jet observations and red histograms are the distributions for the whole magnetosheath data set from which jets are selected. Green histograms (those with error bars) show the probability distributions produced by dividing the jet samples by the corresponding magnetosheath data, as described in Section 2.2.

From the green curve in Figure 3a, we see that jet formation is highest during low IMF cone angle solar wind. This is in agreement with the findings of Plaschke et al. (2013) who, with their smaller data set, concluded that cone angle was the only strongly controlling factor, but noted weak dependencies on density and wind speed. Low IMF $|B|$ (Figure 3c), high β (Figure 3d), low dynamic pressure (Figure 3e), and high Alfvén Mach number (Figure 3f), also appear to promote jet formation. From Figure 3g it does indeed appear that jets are more likely to form during low density wind, arguably displaying a more than minor dependence. The results for Alfvén Mach number and β are in agreement with the recent conclusions of Goncharov et al. (2020), though they found the opposite result for the IMF magnitude. It should be noted, however, that their data set was significantly smaller (1,400 jets) than this present study, and they did not distinguish between formation and propagation effects. We see jet formation probability as a function of solar wind speed (Figure 3b) to display an interesting shape with a significant dip around 350–500 $\mathrm{km\,s^{-1}}$. This pattern is not dissimilar to what was seen by Archer and Horbury (2013), particularly downstream of the quasi-parallel shock. We find that for our magnetosheath data set, large ($> 10\,\mathrm{nT}$) values of IMF magnitude occur most often when the solar wind speed is around $400\,\mathrm{km\,s^{-1}}$ (not shown). The corresponding trend is also reflected in the related dimensionless quantities, Alfvén Mach number and β. I.e., low M_A and β are relatively more frequent during intermediate solar wind velocities. As established from Figure 3c, high IMF $|B|$ decreases the probability of jet formation, and so do low M_A and β. Consequently, at this 350–500 $\mathrm{km\,s^{-1}}$ solar wind speed range the associated high IMF magnitude decreases the likelihood of jet formation, modulating the distribution and causing the observed dip in the probability distribution. It is also interesting to note that this signature is only seen near the bow shock. Replicating the analysis with near-magnetopause jets, which we show in the following subsection, or the whole jet data set results in only the peak at high speeds. This illustrates the need to disentangle jet formation and propagation effects.

3.2 Factors Affecting Jet Propagation

Figure 4 shows the results of the first technique (Figure 2b) used to determine the effect of solar wind conditions on jet propagation. The overlaid histograms show the dis-

3.pdf

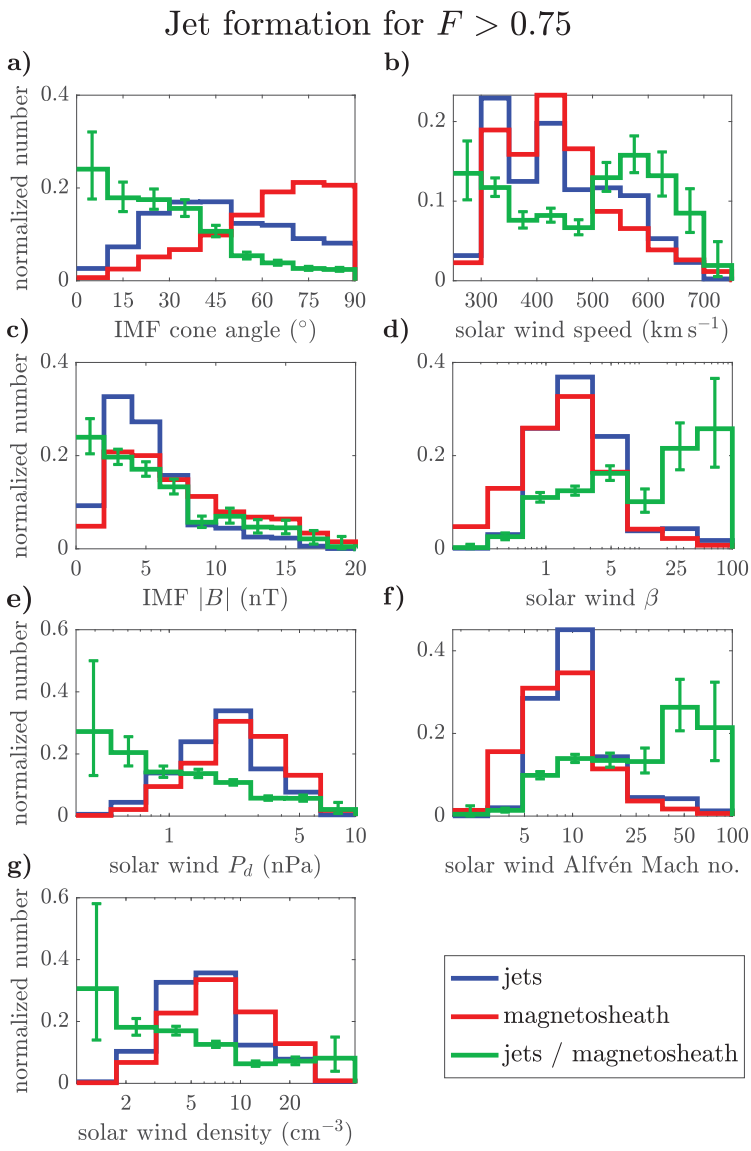


Figure 3. Distributions of upstream solar wind conditions, illustrating how they affect the probability of jets forming at the bow shock. Observations associated with jets are shown in blue, the whole magnetosheath data set in red, and the normalized probability distributions for jet formation (those with error bars) in green. All observations are restricted to $F > 0.75$, i.e., near the bow shock, corresponding to the green region of Figure 2. Solar wind quantities shown are: a) IMF cone angle; b) solar wind speed; c) IMF magnitude; d) solar wind plasma β (log scale); e) solar wind dynamic pressure (log scale); f) solar wind Alfvén Mach number (log scale); g) solar wind density (log scale).

4.pdf

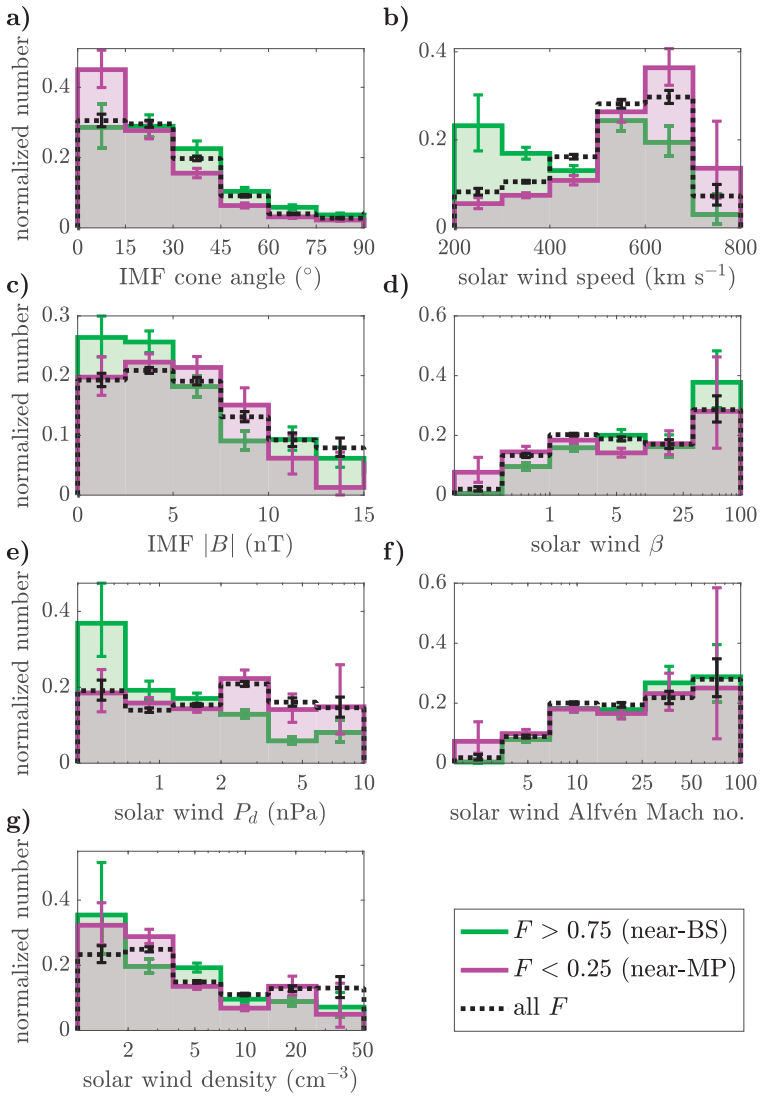


Figure 4. Distributions of upstream solar wind properties for jets, separated by near-bow shock ($F > 0.75$, green) and near-magnetopause ($F < 0.25$, magenta) jets. Distribution for all F values shown with a black dotted line. a) IMF cone angle; b) solar wind speed; c) IMF magnitude; d) solar wind plasma β (log scale); e) solar wind dynamic pressure (log scale); f) solar wind Alfvén Mach number (log scale); g) solar wind density (log scale).

tributions of solar wind parameters for jets observed close to the magnetopause ($F < 0.25$, magenta) of which there are 1,924, compared with jets observed near the bow shock ($F > 0.75$, green) of which there are 1,739 (Table 1). The colors indicate correspondence with the green and magenta regions of Figure 2a. IMF cone angle (Figure 4a) appears to be a controlling factor for jet propagation, with jets observed near the magnetopause showing an even stronger preference to occur during low cone angles than near-bow shock jets. Solar wind speed (Figure 4b) shows a very clear split, with jets observed near the bow shock recording far slower upstream solar wind speeds than jets near the magnetopause, implying that jets formed during faster wind will be more likely to reach the magnetopause. The distributions in Figures 4c, 4d, 4f, and 4g, representing IMF magnitude, plasma β, Alfvén Mach number, and density, respectively, lie roughly on top of each other, overlapping in their error bars and showing no clear skew. This suggests that, within uncertainty, they have no effect on jet propagation. Figure 4e, showing solar wind dynamic pressure, indicates that jets observed near the bow shock are generally formed of low dynamic pressure solar wind while jets at the magnetopause are formed from a range of dynamic pressures. This creates a separation in the upper region of the scale, suggesting that high dynamic pressure solar wind creates jets more likely to reach the magnetopause. This is compatible with the clear dependence on solar wind speed.

Figure 5 shows jet F distributions separated by high and low values (the 85^{th} and 15^{th} percentiles) of each solar wind parameter, our second technique used to investigate jet propagation (Figure 2c). In each, orange histograms show high solar wind values, while cyan regions show low values, where the colors once again correspond to the regions highlighted in Figure 2a. The potential factors identified in the previous subsection — low IMF cone angle (Figure 5a), high solar wind speed (Figure 5b), and high dynamic pressure (Figure 5e) — all show clear confirmation of their influence, with the two distributions showing clear separation. Figure 5a provides a broader statistical backing for the assertion made by Goncharov et al. (2020) that jets propagate further into the magnetosheath downstream of the quasi-parallel shock. In addition, Figures 5c and 5d suggest that, according to this analysis technique, higher IMF $|B|$ and low solar wind β may in fact promote jet propagation. These factors did not produce a noticeable effect via the first technique. The Alfvén Mach number and solar wind density (Figures 5f and 5g) do not show a clear effect.

4 Discussion

Thus far we have considered the solar wind control of jet formation and jet propagation separately. For example, we have seen that a low IMF magnitude is favorable for the creation of jets (Figure 3c), but also that a higher IMF magnitude increases the likelihood of a jet surviving from the bow shock to the magnetopause (Figure 5c). On first glance, these two statements may seem contradictory but it is in fact possible for a solar wind parameter to affect jet formation and propagation differently. However, our results so far give us no information as to the relative magnitudes of these effects, or which regime might dominate. To address this, we present Figure 6 which, like Figure 5, shows F distributions separated by high and low threshold values of each solar wind parameter. The key difference here, however, is that, instead of simply normalizing, we express histograms in units of jets observed per hour the spacecraft spent in the magnetosheath, within each F bin, under those solar wind conditions. This combines both formation and propagation effects, enabling us to extract the rates of jets reaching the magnetopause under different solar wind conditions. The dashed black curves show the F distributions unconstrained by solar wind conditions and are therefore representative of the black curve in Figure 1c (though with different binwidth). This allows us to see how each jet subset observed under constrained solar wind conditions compares to the general population, and the factors that most strongly contribute to the shape of the curve. Note also that by comparing the left side of each plot (in particular for $0.75 < F < 1$) we can

5.pdf

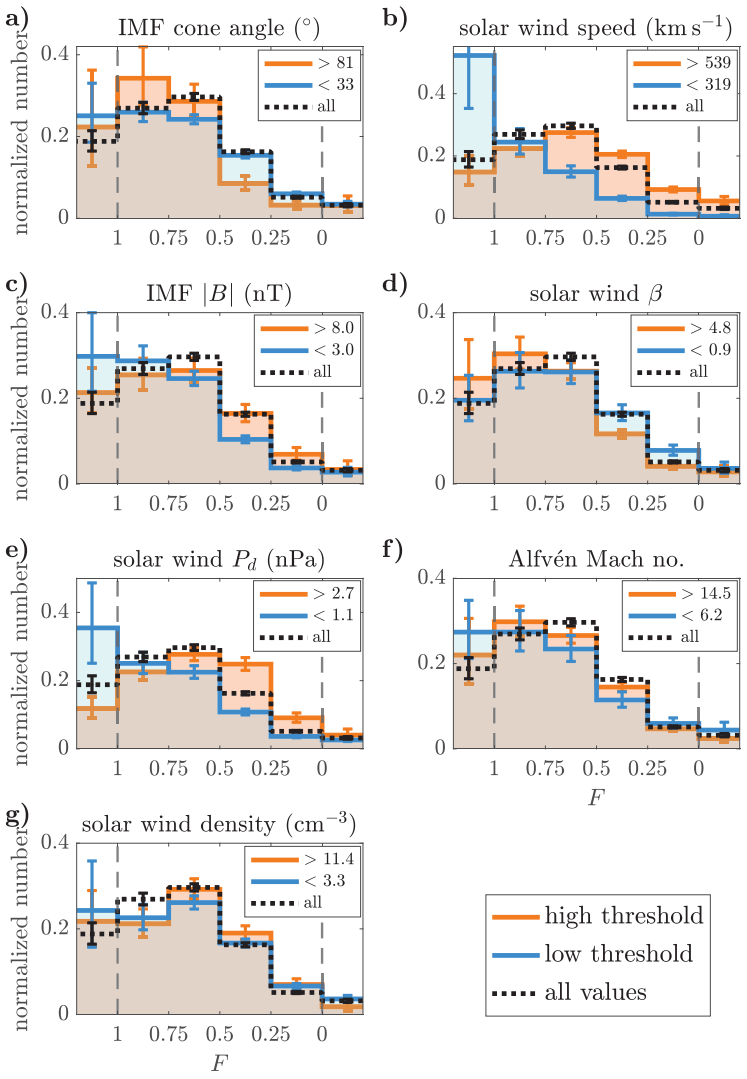


Figure 5. Normalized distributions of jet observation locations in model magnetosheath, separated by high and low threshold values (the 85$^{\text{th}}$ and 15$^{\text{th}}$ percentiles) of upstream solar wind parameters. In each, orange histograms are for jets observed with solar wind conditions above a high threshold, while cyan distributions represent those below a low threshold. Unconstrained distributions are shown with a black dotted line. a) IMF cone angle; b) solar wind speed; c) IMF magnitude; d) solar wind plasma β; e) solar wind dynamic pressure; f) solar wind Alfvén Mach number; g) solar wind density.

clearly see the factors influencing jet formation rates at the bow shock (as explored in Figure 3).

The cyan histogram in Figure 6a, representing low cone angles, dwarfs its high cone angle counterpart throughout all regions of the magnetosheath showing that, as expected from the preceding results, jets are far more likely to reach the magnetopause under low cone angle solar wind than high cone angle solar wind. A similar, but not as strong, combined effect is seen for solar wind speed in Figure 6b. Quantities that display oppositely directed formation and propagation effects are particularly interesting. In Figure 6c we can see that for low IMF magnitude solar wind there are significantly more jets formed at the bow shock. However, due to the propagation effects described in Section 3.2, the observation rate falls far faster than the high IMF magnitude solar wind such that near the magnetopause the occurrence rate of jets formed from low IMF magnitude solar wind is only marginally higher than for high IMF magnitudes. This cancellation effect is even clearer in solar wind plasma β (Figure 6d) and dynamic pressure (Figure 6g), and so both can be said to have no overall effect on the rate of jets reaching the magnetopause.

In Table 2 we quantify these effects and give numerical comparisons of jet observation rates at the magnetopause for high and low values of each solar wind parameter. The multiplication factor is drawn from the difference in height of the $0 < F < 0.25$ bars in each panel of Figure 6. The numbers of near-magnetopause jets contributing to the calculation of the multiplication factor are also shown in Table 2. Note that we do not place emphasis on the absolute values in jets per hour (though these can be read from Figure 6), as our selection criteria are such that smaller jets are more likely to be missed (Plaschke, Hietala, & Vörös, 2020), and our observation window is confined to the subsolar region. However, the relative observation rates under different solar wind conditions give clear indicators as to what factors are most relevant for magnetopause impacts. We therefore provide quantitative estimates for how the changing solar wind conditions affect the likelihood of jets reaching the magnetopause. IMF cone angle is the strongest controlling factor overall, with over 17 times as many jets expected to reach the magnetopause under low ($< 33°$) angles than under high ($> 81°$) angles. This factor is more extreme than the factor of 9 disparity in jet occurrence rate observed by Vuorinen et al. (2019) due to the compounding of formation and propagation effects. The next largest is solar wind speed, where we see 8.3 times as many jets in front of the magnetopause when the solar wind is fast ($> 539\,\mathrm{km\,s^{-1}}$) compared to when it is slow ($< 319\,\mathrm{km\,s^{-1}}$). The influences of low IMF magnitude, high Alfvén Mach number, and low density are more minor in comparison but still notable, each making jet impacts approximately twice as likely as their opposite conditions. This analysis is somewhat sensitive to the exact values chosen to define 'high' and 'low' thresholds. A variety of percentile thresholds were considered and tested, which produced minor changes in the multiplication factors calculated, meaning that the values shown in the last column of Table 2 should be taken as approximate indicators of the scale of each effect. The general conclusions, however, remain intact regardless of the choice of threshold values, with IMF cone angle always being the strongest controlling factor, followed by solar wind speed, then density. The only parameters examined in this study that show no clear net effect on the likelihood of jets reaching the magnetopause are the solar wind dynamic pressure and plasma β.

Our analysis is subject to some limitations and caveats. If jets are braked during propagation, they may be slowed to the point that they are no longer detectable via our jet selection criteria (that their earthward dynamic pressure exceeds half that of the pristine solar wind). This, in part, may explain the drop-off that is seen in the black curves of Figure 1, potentially exaggerating the gradient if a number of weakened jets continue to propagate undetected. Similarly, Plaschke, Hietala, and Vörös (2020) suggested that jets can fragment into several smaller jets (or merge into larger ones) as they travel, changing their cross-sectional areas, and thus the likelihood of being observed by a single spacecraft. This raises questions about where is an appropriate level to set the detection thresh-

6.pdf

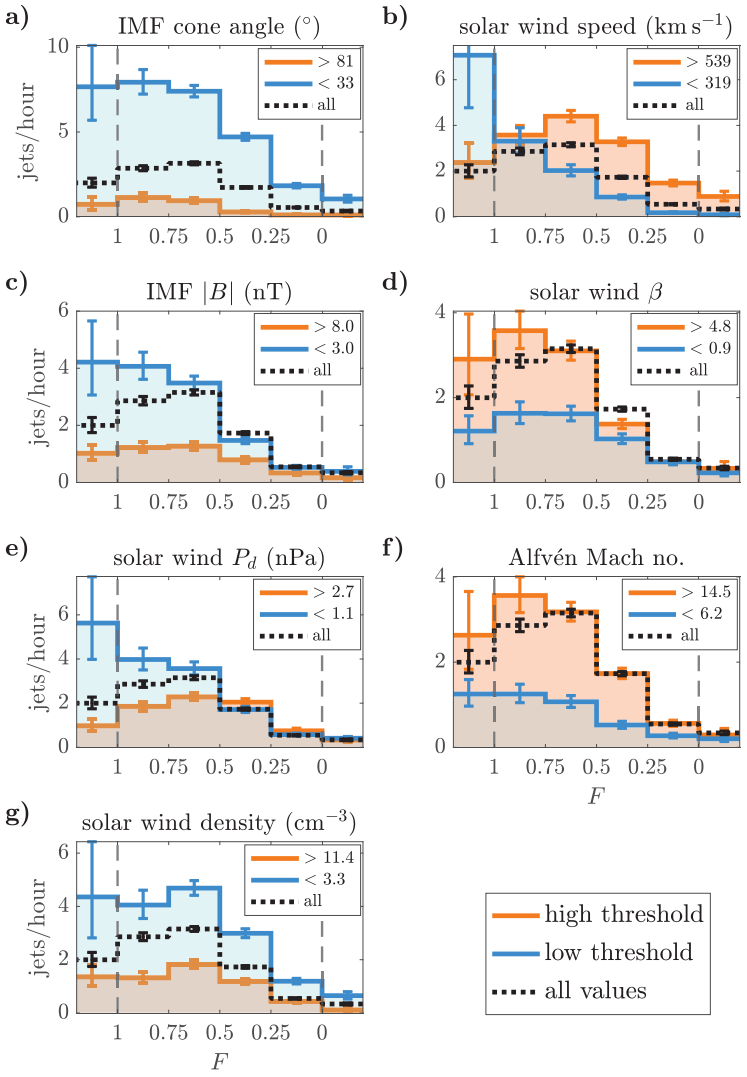


Figure 6. Same format as Figure 5 except that distributions are expressed in units of jets per hour per bin spent in the magnetosheath for each restricted distribution, thus combining formation and propagation effects. The net effect on the number of jets reaching the magnetopause is calculated from the $0 < F < 0.25$ bin. a) IMF cone angle; b) solar wind speed; c) IMF magnitude; d) solar wind plasma β; e) solar wind dynamic pressure; f) solar wind Alfvén Mach number; g) solar wind density.

Table 2. Summary of effects of solar wind conditions on the numbers of jets expected to reach the magnetopause.

Solar wind parameter	High	Low	Jets (high)	Jets (low)	Multiplication factor
Cone angle (°)	>81	<33	48	778	17.3 (low)
Speed ($km\,s^{-1}$)	>539	<319	533	106	8.3 (high)
IMF $\lvert B\rvert$ (nT)	>8.0	<3.0	90	250	1.6 (low)
β	>4.8	<0.9	224	174	No net effect
Dynamic Pressure (nPa)	>2.7	<1.1	176	326	No net effect
Alfvén Mach number	>14.5	<6.2	241	98	2.1 (high)
Density (cm^{-3})	>11.4	<3.3	126	520	2.7 (low)

Note. All statistics derived from jet observations with $0 < F < 0.25$, i.e., immediately in front of the magnetopause. Threshold values given in columns 2 and 3 are those used to define 'high' and 'low' populations in Figures 5 and 6, i.e., 85^{th} and 15^{th} percentiles of each solar wind parameter in the full magnetosheath data set. Columns 4 and 5 give the number of jets in the $0 < F < 0.25$ bin (in front of the magnetopause) under each constrained solar wind condition. The multiplication factor in column 6 is calculated as the ratio of jets expected at the magnetopause per hour under differing solar wind parameters. 'High' and 'low' indicate which regime is dominant in each case.

old, i.e., how small or slow does a jet have to become before it is no longer considered a jet? While an interesting problem, we do not consider it an issue as the focus of this study is understanding the conditions most relevant for magnetopause impacts. We are, therefore, most interested in larger and faster jets observed near the magnetopause, i.e., those with a greater chance of being geoeffective, which our selection criteria are most likely to capture. Note also that we do not observe jets actually impacting the magnetopause. However, we find it reasonable to assume that a jet observed immediately in front of the magnetopause will later go on to strike it. We propose that a dedicated study of magnetopause crossings should be performed to build a database of jet impacts and catalog their effects on the surrounding plasma environment.

A potential explanation for higher solar wind dynamic pressures increasing the likelihood of jets propagating far into the magnetosheath can be reached by considering jet travel times. Under high dynamic pressure conditions, the magnetosheath layer is compressed and thinned, decreasing the time taken for a jet to reach the magnetopause. Similarly, we see that higher solar wind speed creates faster jets (though this is, to an extent, necessitated by our selection criteria), which are then able to reach the magnetopause in less time. This could lower the chance of a jet being broken up, though it is unlikely to be the only factor affecting the dissipation rate. Further study should, therefore, be conducted into how jets interact with instabilities and dissipation mechanisms. Analytical modeling by Hietala and Plaschke (2013) found that low β solar wind produces jets with higher dynamic pressure relative to the upstream solar wind. This would likely increase their ability to propagate far into the magnetosheath, which is in line with our observations (Figure 5d). They also saw stronger jets during high Alfvén Mach solar wind, however we see little evidence for high Alfvén Mach solar wind increasing jet propagation (Figure 5f). This may be explained by the simulation study by Omidi et al. (2016), where in high Alfvén Mach solar wind regimes, increased turbulence within the magnetosheath inhibited the propagation of jets and decreased their size.

Many of the solar wind properties studied are related. Fast solar wind is generally expected to have a lower density and a more radial magnetic field (i.e., lower cone angle), though it is generally seen to have a lower Alfvén Mach number than slow solar wind (see, e.g, Ebert et al., 2009). As fast solar wind is seen at the equator more often in times

near solar maximum (e.g., McComas et al., 2003) there may therefore be a solar cycle dependence for jets impacting the magnetopause. This may explain the differences between the two data sets in terms of jet occurrence rates and distributions in F (i.e., between Figure 1a and 1b), as the former was compiled around a deep solar minimum, while the latter included solar maximum.

Our results also suggest that it may be interesting to study magnetosheath jets as a response to extreme solar wind transients. Coronal mass ejections (CMEs) are typically observed with higher speeds, densities, and magnetic field magnitudes than the ambient solar wind at 1 AU (e.g., Kilpua et al., 2017). Based on our findings, CMEs may enhance the rates of jets reaching the magnetopause by virtue of their speed, though increased density may work to counteract this. Increased magnetic field strength may reduce the absolute numbers of jets formed at the bow shock, but the likelihood of their survival to the magnetopause will be increased such that the rates of jets reaching the magnetopause are largely unaffected by the magnetic field magnitude itself. The potential effects may even extend beyond those arising directly from the magnetic cloud itself. Neugebauer et al. (1997) observed that extended periods of radial IMF often follow in the wake of a CME. This idea sets up an interesting scenario where jet production and propagation could be increased both during a CME impact and in the hours following it.

Analysis by Turc et al. (2018, 2019) showed through global simulations and Cluster observations that a higher IMF $|B|$ causes foreshock waves to move to smaller spatial scales, which in turn creates smaller ripples on the quasi-parallel bow shock, increasing the number of potential sites for jet formation. Our results appear in contradiction to this, where we see that higher magnetic field magnitudes actually decrease the likelihood of jet formation (Figure 3c). However it may be the case that smaller ripples create more, but smaller, jets that are less likely to be detected by a single spacecraft. More targeted research into the effects of CMEs on magnetosheath jets is needed. Naturally, this also applies to other solar wind transients such as stream interaction regions (SIRs) and corotating interaction regions (CIRs) that present increased speeds and so would also be expected to have an effect on the rate of jet production and propagation (Jian et al., 2006).

5 Summary and Conclusion

Using a new database of 13,096 jets seen by the THEMIS spacecraft from 2008 to 2018 we have performed statistical analysis to determine how upstream solar wind conditions (obtained from OMNI) affect the likelihood of jets forming at the bow shock and then propagating to the magnetopause without dissipating. We find that a number of parameters increase the likelihood of jets forming at the bow shock, the most favorable conditions being: low IMF cone angle, solar wind speeds of $\sim 300\,\mathrm{km\,s^{-1}}$ or $\sim 600\,\mathrm{km\,s^{-1}}$, low IMF magnitude, high β, low dynamic pressure, high Alfvén Mach number, and low density. We find that once jets are formed at the bow shock, their likelihood of surviving throughout propagation to the magnetopause is also controlled by the upstream solar wind conditions. The conditions most favorable for this are: low IMF cone angle, high solar wind speed, high IMF magnitude, low β, and high dynamic pressure. Combining these two effects, we find that higher numbers of jets reach, and therefore likely impact, the magnetopause when the solar wind exhibits a low IMF cone angle, high wind speed, high Alfvén Mach number, and low density. Solar wind β and dynamic pressure display no net effect on the rates of jets reaching the magnetopause.

It is notable that several of these properties are associated with fast solar wind and extreme solar wind transient events, and therefore may be modulated by the solar cycle. Under these solar wind conditions the highest impact rates of jets on the magnetopause are expected, increasing the likelihood of them affecting magnetospheric dynamics and

potentially inducing space weather effects. Many opportunities for future work are apparent. We suggest a targeted study on the relation of jets and solar wind transients be performed, as well as further investigation into the properties of near-magnetopause jets and their interactions with the magnetopause. We hope that these findings will provide a useful step towards eventual space weather forecasting regimes whereby we will be able to predict the inner-magnetosphere effects of magnetosheath jets purely from measurements of the solar wind upstream of the bow shock.

Acknowledgments

ATL and HH were supported by Royal Society awards URF\R1\180671 and RGF\EA\181090. FP was supported by the Austrian Science Fund (FWF): P 33285-N. LV acknowledges the financial support of the Academy of Finland (Project #309939) and of the University of Turku Graduate School. JPE was supported by UKRI/STFC grant ST/S000364/1. THEMIS and OMNI data can be accessed using the SPEDAS software (Angelopoulos et al., 2019). Jet and magnetosheath interval times are available at `https://osf.io/gf732/` (2008–2011; Plaschke, Hietala, & Angelopoulos, 2020) and `https://osf.io/7rjs4/` (2012–2018; Plaschke, Hietala, & LaMoury, 2020).

References

Amata, E., Savin, S., Ambrosino, D., Bogdanova, Y., Marcucci, M., Romanov, S., & Skalsky, A. (2011). High kinetic energy density jets in the earth's magnetosheath: A case study. *Planetary and Space Science*, *59*(7), 482 - 494. doi: 10.1016/j.pss.2010.07.021

Angelopoulos, V. (2008). The THEMIS mission. *Space Science Reviews*, *141*(1-4), 5–34. doi: 10.1007/s11214-008-9336-1

Angelopoulos, V., Cruce, P., Drozdov, A., Grimes, E. W., Hatzigeorgiu, N., King, D. A., ... Schroeder, P. (2019). The Space Physics Environment Data Analysis System (SPEDAS). *Space Science Reviews*, *215*(1), 9. doi: 10.1007/s11214-018-0576-4

Archer, M. O., Hietala, H., Hartinger, M. D., Plaschke, F., & Angelopoulos, V. (2019). Direct observations of a surface eigenmode of the dayside magnetopause. *Nature Communications*, *10*(1), 615. doi: 10.1038/s41467-018-08134-5

Archer, M. O., & Horbury, T. S. (2013). Magnetosheath dynamic pressure enhancements: Occurrence and typical properties. *Annales Geophysicae*, *31*(2), 319–331. doi: 10.5194/angeo-31-319-2013

Archer, M. O., Horbury, T. S., & Eastwood, J. P. (2012). Magnetosheath pressure pulses: Generation downstream of the bow shock from solar wind discontinuities. *Journal of Geophysical Research: Space Physics*, *117*(5), 1–13. doi: 10.1029/2011JA017468

Archer, M. O., Turner, D. L., Eastwood, J. P., Horbury, T. S., & Schwartz, S. J. (2014). The role of pressure gradients in driving sunward magnetosheath flows and magnetopause motion. *Journal of Geophysical Research: Space Physics*, *119*(10), 8117–8125. doi: 10.1002/2014JA020342

Brown, L. D., Cai, T. T., & DasGupta, A. (2001). Interval estimation for a binomial proportion. *Statistical Science*, *16*(2), 101 – 133. doi: 10.1214/ss/1009213286

Burch, J. L., Moore, T. E., Torbert, R. B., & Giles, B. L. (2016). Magnetospheric Multiscale overview and science objectives. *Space Science Reviews*, *199*(1-4), 5–21. doi: 10.1007/s11214-015-0164-9

Dmitriev, A. V., & Suvorova, A. V. (2012). Traveling magnetopause distortion related to a large-scale magnetosheath plasma jet: THEMIS and ground-based observations. *Journal of Geophysical Research: Space Physics*, *117*(8), 1–16. doi: 10.1029/2011JA016861

Dmitriev, A. V., & Suvorova, A. V. (2015). Large-scale jets in the magnetosheath and plasma penetration across the magnetopause: Themis observations. *Journal of Geophysical Research: Space Physics*, *120*(6), 4423-4437. doi: 10.1002/2014JA020953

Ebert, R. W., McComas, D. J., Elliott, H. A., Forsyth, R. J., & Gosling, J. T. (2009). Bulk properties of the slow and fast solar wind and interplanetary coronal mass ejections measured by Ulysses: Three polar orbits of observations. *Journal of Geophysical Research: Space Physics*, *114*(1). doi: 10.1029/2008JA013631

Goncharov, O., Gunell, H., Hamrin, M., & Chong, S. (2020). Evolution of High-Speed Jets and Plasmoids Downstream of the Quasi-Perpendicular Bow Shock. *Journal of Geophysical Research: Space Physics*, *125*(6), 1–16. doi: 10.1029/2019JA027667

Han, D.-S., Liu, J.-J., Chen, X.-C., Xu, T., Li, B., Hu, Z.-J., ... Pollock, C. J. (2018). Direct evidence for throat aurora being the ionospheric signature of magnetopause transient and reflecting localized magnetopause indentations. *Journal of Geophysical Research: Space Physics*, *123*(4), 2658-2667. doi: 10.1002/2017JA024945

Hietala, H., Laitinen, T. V., Andréeová, K., Vainio, R., Vaivads, A., Palmroth, M., ... Rème, H. (2009). Supermagnetosonic jets behind a collisionless quasiparallel shock. *Physical Review Letters*, *103*(24), 20–23. doi: 10.1103/PhysRevLett.103.245001

Hietala, H., Partamies, N., Laitinen, T. V., Clausen, L. B., Facskò, G., Vaivads, A., ... Lucek, E. A. (2012). Supermagnetosonic subsolar magnetosheath jets and their effects: From the solar wind to the ionospheric convection. *Annales Geophysicae*, *30*(1), 33–48. doi: 10.5194/angeo-30-33-2012

Hietala, H., Phan, T. D., Angelopoulos, V., Oieroset, M., Archer, M. O., Karlsson, T., & Plaschke, F. (2018). In Situ Observations of a Magnetosheath High-Speed Jet Triggering Magnetopause Reconnection. *Geophysical Research Letters*, *45*(4), 1732–1740. doi: 10.1002/2017GL076525

Hietala, H., & Plaschke, F. (2013). On the generation of magnetosheath high-speed jets by bow shock ripples. *Journal of Geophysical Research: Space Physics*, *118*(11), 7237–7245. doi: 10.1002/2013JA019172

Jian, L., Russell, C. T., Luhmann, J. G., & Skoug, R. M. (2006). Properties of Stream Interactions at One AU During 1995 – 2004. *Solar Physics*, *239*(1), 337–392. doi: 10.1007/s11207-006-0132-3

Karimabadi, H., Roytershteyn, V., Vu, H. X., Omelchenko, Y. A., Scudder, J., Daughton, W., ... Geveci, B. (2014). The link between shocks, turbulence, and magnetic reconnection in collisionless plasmas. *Physics of Plasmas*, *21*(6). doi: 10.1063/1.4882875

Karlsson, T., Kullen, A., Liljeblad, E., Brenning, N., Nilsson, H., Gunell, H., & Hamrin, M. (2015). On the origin of magnetosheath plasmoids and their relation to magnetosheath jets. *Journal of Geophysical Research A: Space Physics*, *120*(9). doi: 10.1002/2015JA021487

Kilpua, E. K., Balogh, A., von Steiger, R., & Liu, Y. D. (2017). Geoeffective Properties of Solar Transients and Stream Interaction Regions. *Space Science Reviews*, *212*(3-4), 1271–1314. doi: 10.1007/s11214-017-0411-3

King, J. H., & Papitashvili, N. E. (2005). Solar wind spatial scales in and comparisons of hourly Wind and ACE plasma and magnetic field data. *Journal of Geophysical Research: Space Physics*, *110*(A2), 1–9. doi: 10.1029/2004JA010649

Liu, T. Z., Hietala, H., Angelopoulos, V., Omelchenko, Y., Vainio, R., & Plaschke, F. (2020). Statistical Study of Magnetosheath Jet-Driven Bow Waves. *Journal of Geophysical Research: Space Physics*, *125*(7), 1–14. doi: 10.1029/2019JA027710

Liu, Z.-Q., Lu, J. Y., Wang, C., Kabin, K., Zhao, J. S., Wang, M., ... Zhao, M. X. (2015). A three-dimensional high Mach number asymmetric magnetopause model from global MHD simulation. *Journal of Geophysical Research: Space Physics*, *120*(7), 5645-5666. doi: 10.1002/2014JA020961

McComas, D. J., Elliott, H. A., Schwadron, N. A., Gosling, J. T., Skoug, R. M., & Goldstein, B. E. (2003). The three-dimensional solar wind around solar maximum. *Geophysical Research Letters*, *30*(10), 1–4. doi: 10.1029/2003gl017136

Merka, J., Szabo, A., Slavin, J. A., & Peredo, M. (2005). Three-dimensional position and shape of the bow shock and their variation with upstream Mach numbers and interplanetary magnetic field orientation. *Journal of Geophysical Research: Space Physics*, *110*(A4). doi: 10.1029/2004JA010944

Neugebauer, M., Goldstein, R., & Goldstein, B. E. (1997). Features observed in the trailing regions of interplanetary clouds from coronal mass ejections. *Journal of Geophysical Research A: Space Physics*, *102*(A9), 19743–19751. doi: 10.1029/97JA01651

Nykyri, K., Bengtson, M., Angelopoulos, V., Nishimura, Y., & Wing, S. (2019). Can Enhanced Flux Loading by High-Speed Jets Lead to a Substorm? Multipoint Detection of the Christmas Day Substorm Onset at 08:17 UT, 2015. *Journal of Geophysical Research: Space Physics*, *124*(6), 4314–4340. doi: 10.1029/2018JA026357

Omidi, N., Berchem, J., Sibeck, D., & Zhang, H. (2016). Impacts of spontaneous hot flow anomalies on the magnetosheath and magnetopause. *Journal of Geophysical Research: Space Physics*, *121*(4), 3155-3169. doi: 10.1002/2015JA022170

Palmroth, M., Hietala, H., Plaschke, F., Archer, M., Karlsson, T., Blanco-Cano, X., ... Turc, L. (2018). Magnetosheath jet properties and evolution as determined by a global hybrid-Vlasov simulation. *Annales Geophysicae*, *36*(5), 1171–1182. doi: 10.5194/angeo-36-1171-2018

Palmroth, M., Raptis, S., Suni, J., Karlsson, T., Turc, L., Johlander, A., ... Osmane, A. (2021). Magnetosheath jet evolution as a function of lifetime: global hybrid-vlasov simulations compared to mms observations. *Annales Geophysicae*, *39*(2), 289–308. doi: 10.5194/angeo-39-289-2021

Plaschke, F., Glassmeier, K. H., Sibeck, D. G., Auster, H. U., Constantinescu, O. D., Angelopoulos, V., & Magnes, W. (2009). Magnetopause surface oscillation frequencies at different solar wind conditions. *Annales Geophysicae*, *27*(12), 4521–4532. doi: 10.5194/angeo-27-4521-2009

Plaschke, F., Hietala, H., & Angelopoulos, V. (2013). Anti-sunward high-speed jets in the subsolar magnetosheath. *Annales Geophysicae*, *31*(10), 1877–1889. doi: 10.5194/angeo-31-1877-2013

Plaschke, F., Hietala, H., & Angelopoulos, V. (2020, Aug). *Anti-sunward high-speed jets in the subsolar magnetosheath: Data sets.* OSF. Retrieved from `osf.io/gf732`

Plaschke, F., Hietala, H., Angelopoulos, V., & Nakamura, R. (2016). Geoeffective jets impacting the magnetopause. *Journal of Geophysical Research: Space Physics*. doi: 10.1002/2016JA022534

Plaschke, F., Hietala, H., Archer, M., Blanco-Cano, X., Kajdič, P., Karlsson, T., ... Sibeck, D. (2018). Jets Downstream of Collisionless Shocks. *Space Science Reviews*, *214*(5). doi: 10.1007/s11214-018-0516-3

Plaschke, F., Hietala, H., & LaMoury, A. T. (2020, Oct). *THEMIS magnetosheath jet data set 2012-2018.* OSF. Retrieved from `osf.io/7rjs4`

Plaschke, F., Hietala, H., & Vörös, Z. (2020). Scale Sizes of Magnetosheath Jets. *Journal of Geophysical Research: Space Physics*, *125*(9). doi: 10.1029/2020JA027962

Qu, B., Lu, J., Wang, M., Yuan, H., Zhou, Y., & Zhang, H. (2021). Formation of the bow shock indentation: MHD simulation results. *Earth and Planetary Physics*, *5*(3), 259-269. doi: 10.26464/epp2021033

Raptis, S., Karlsson, T., Plaschke, F., Kullen, A., & Lindqvist, P. A. (2020). Classifying Magnetosheath Jets Using MMS: Statistical Properties. *Journal of Geophysical Research: Space Physics*, *125*(11). doi: 10.1029/2019JA027754

Schwartz, S. J., & Burgess, D. (1991). Quasi-parallel shocks: A patchwork of three-dimensional structures. *Geophysical Research Letters*, *18*(3), 373–376. doi: 10.1029/91GL00138

Shue, J.-H., Chao, J. K., Song, P., McFadden, J. P., Suvorova, A., Angelopoulos, V., ... Plaschke, F. (2009). Anomalous magnetosheath flows and distorted subsolar magnetopause for radial interplanetary magnetic fields. *Geophysical Research Letters*, *36*(18), 3–7. doi: 10.1029/2009GL039842

Shue, J.-H., Song, P., Russell, C. T., Steinberg, J. T., Chao, J. K., Zastenker, G., ... Kawano, H. (1998). Magnetopause location under extreme solar wind conditions. *Journal of Geophysical Research: Space Physics*, *103*(A8), 17691–17700. doi: 10.1029/98ja01103

Suvorova, A. V., Shue, J. H., Dmitriev, A. V., Sibeck, D. G., McFadden, J. P., Hasegawa, H., ... Němeček, Z. (2010). Magnetopause expansions for quasi-radial interplanetary magnetic field: THEMIS and Geotail observations. *Journal of Geophysical Research: Space Physics*, *115*(10), 1–16. doi: 10.1029/2010JA015404

Swisdak, M., Opher, M., Drake, J. F., & Alouani Bibi, F. (2010). The vector direction of the interstellar magnetic field outside the heliosphere. *Astrophysical Journal*, *710*(2), 1769–1775. doi: 10.1088/0004-637X/710/2/1769

Turc, L., Ganse, U., Pfau-Kempf, Y., Hoilijoki, S., Battarbee, M., Juusola, L., ... Palmroth, M. (2018). Foreshock Properties at Typical and Enhanced Interplanetary Magnetic Field Strengths: Results From Hybrid-Vlasov Simulations. *Journal of Geophysical Research: Space Physics*, *123*(7), 5476–5493. doi: 10.1029/2018JA025466

Turc, L., Roberts, O. W., Archer, M. O., Palmroth, M., Battarbee, M., Brito, T., ... Dandouras, I. (2019). First Observations of the Disruption of the Earth's Foreshock Wave Field During Magnetic Clouds. *Geophysical Research Letters*, *46*(22), 12644–12653. doi: 10.1029/2019GL084437

Vuorinen, L., Hietala, H., & Plaschke, F. (2019). Jets in the magnetosheath: IMF control of where they occur. *Annales Geophysicae*, *37*(4), 689–697. doi: 10.5194/angeo-37-689-2019

Wang, B., Nishimura, Y., Hietala, H., Lyons, L., Angelopoulos, V., Plaschke, F., ... Weatherwax, A. (2018). Impacts of Magnetosheath High-Speed Jets on the Magnetosphere and Ionosphere Measured by Optical Imaging and Satellite Observations. *Journal of Geophysical Research: Space Physics*, *123*(6), 4879–4894. doi: 10.1029/2017JA024954

Figure 1.

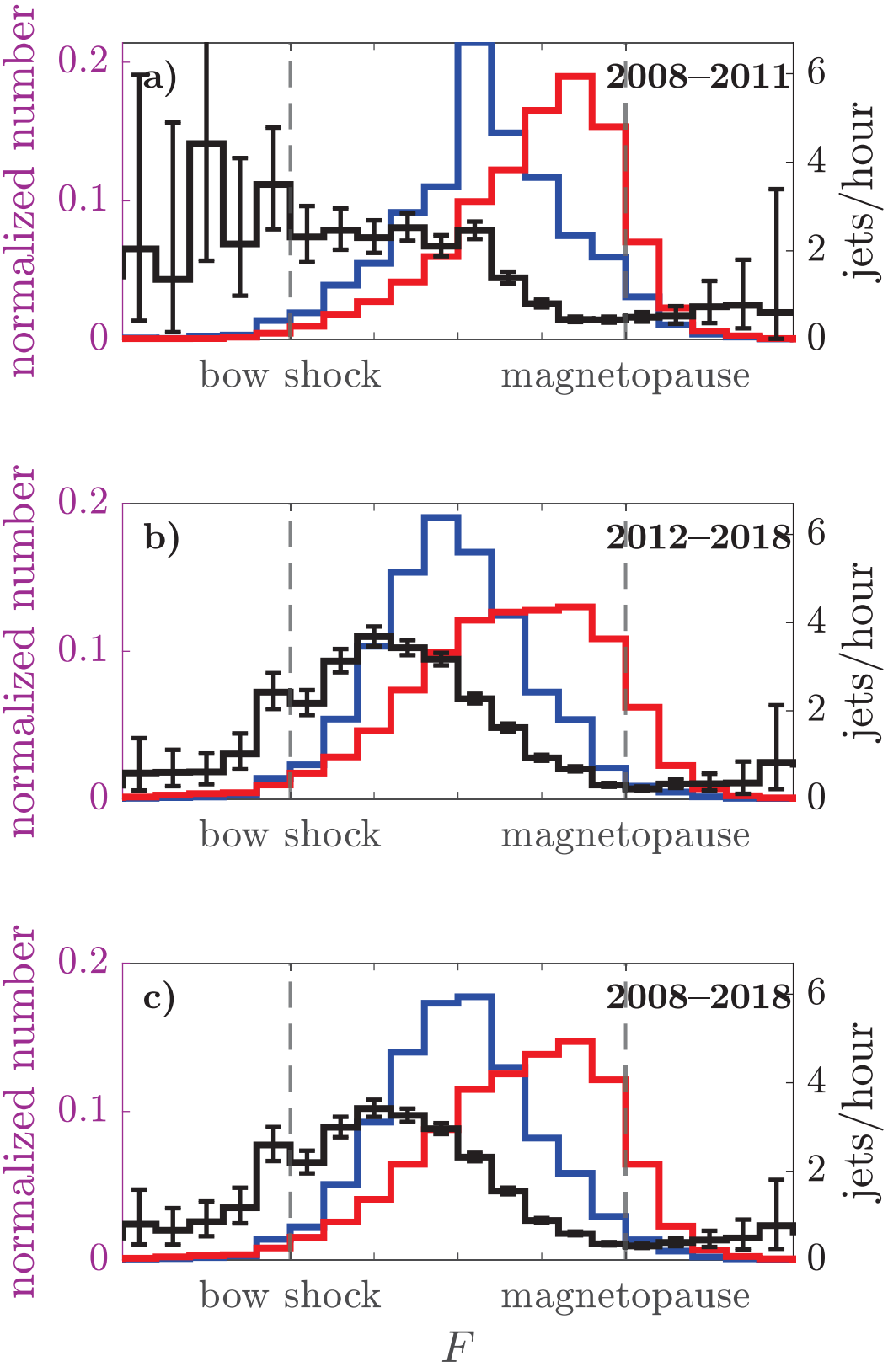

a)
2008–2011
b)
2012–2018
c)
2008–2018
normalized number
jets/hour
0
0.1
0.2
2
4
6
bow shock
magnetopause
F
jets (normalized)
magnetosheath (normalized)
jets / magnetosheath (jets/hour)

Figure 2.

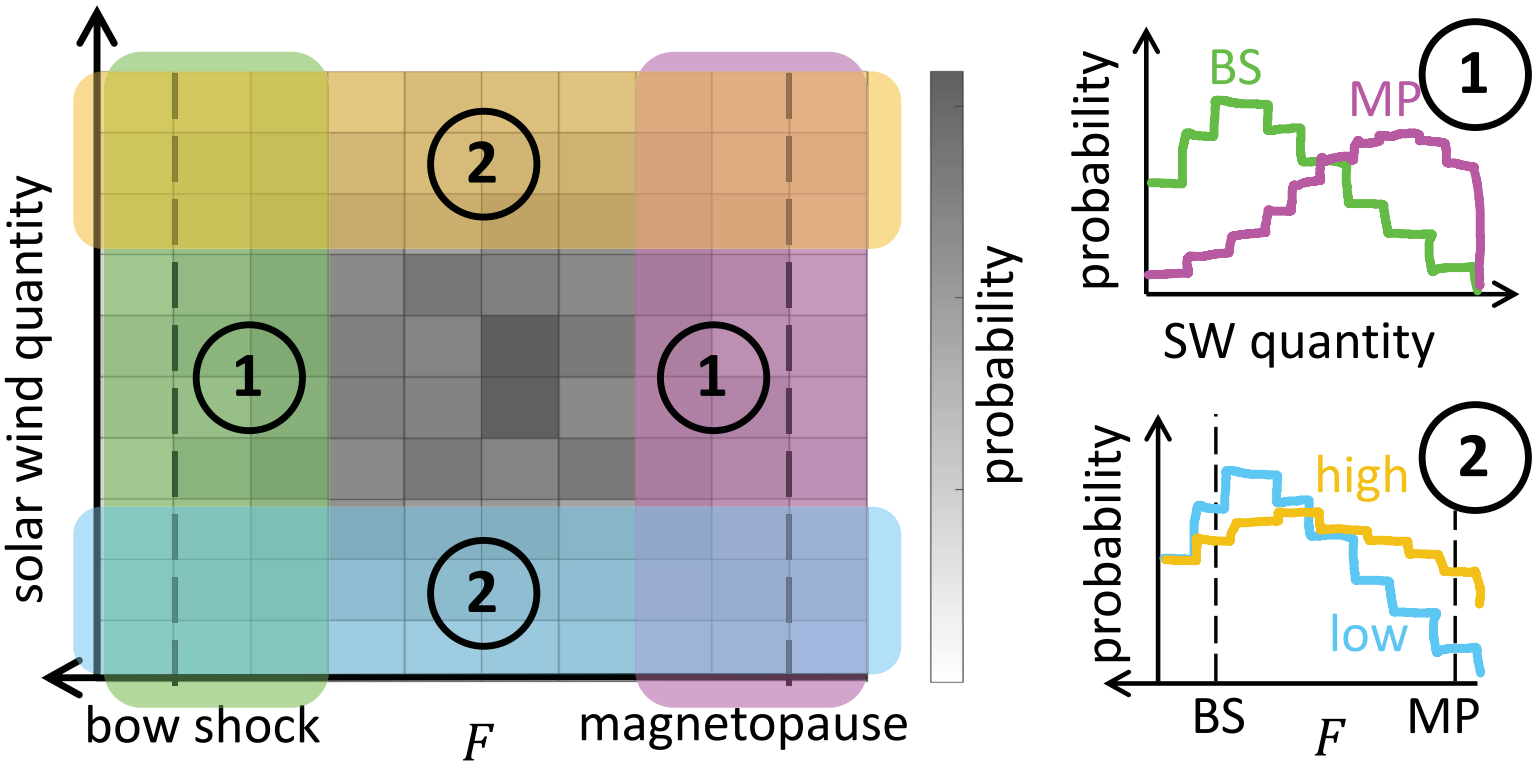

solar wind quantity
bow shock
F
magnetopause
probability
1
2
1
2
probability
BS
MP
1
SW quantity
probability
high
low
2
BS
F
MP

Figure 3.

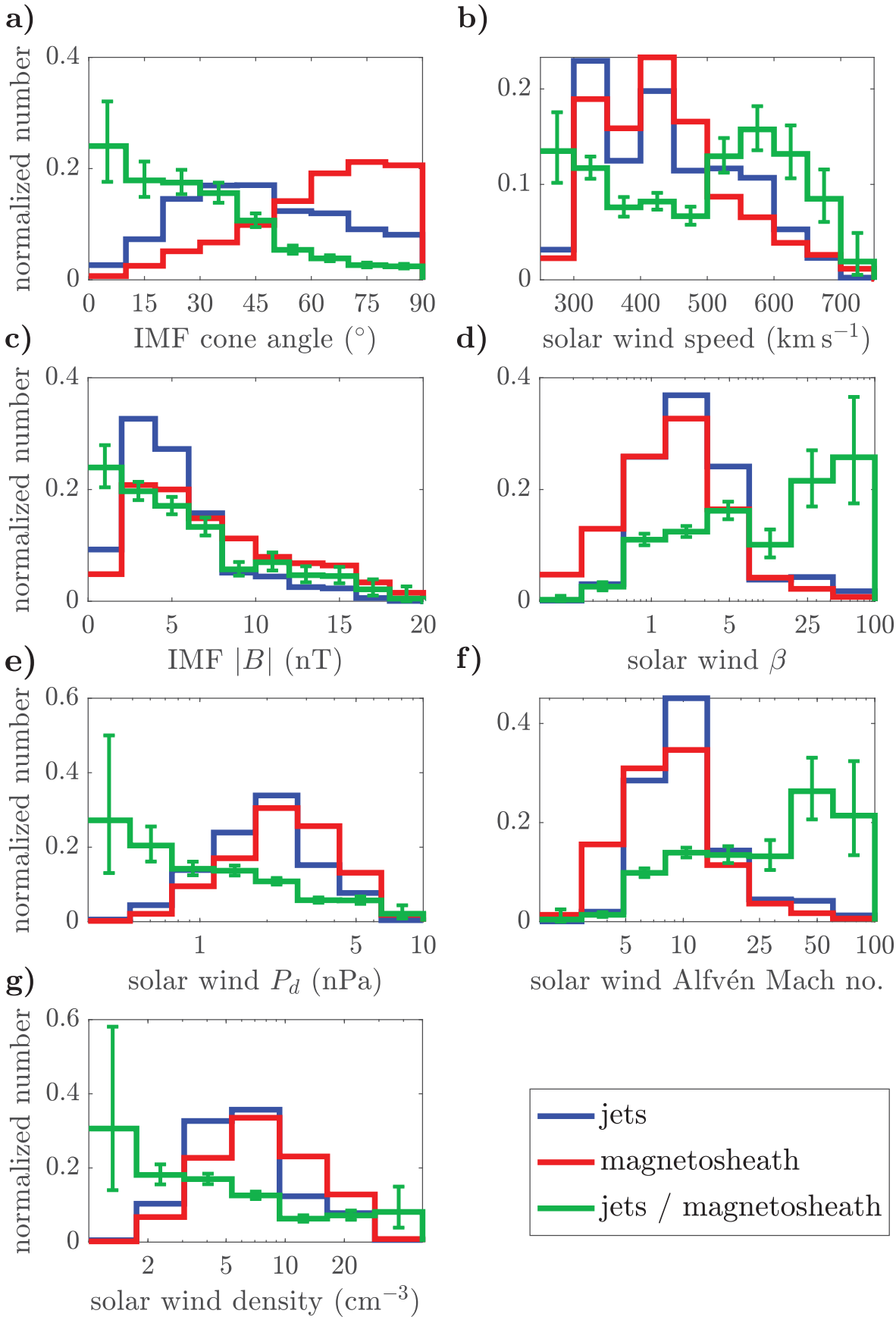

Jet formation for $F > 0.75$
a)
b)
c)
d)
e)
f)
g)
normalized number
IMF cone angle (°)
solar wind speed (km s^{-1})
IMF $|B|$ (nT)
solar wind β
solar wind P_d (nPa)
solar wind Alfvén Mach no.
solar wind density (cm^{-3})
jets
magnetosheath
jets / magnetosheath

Figure 4.

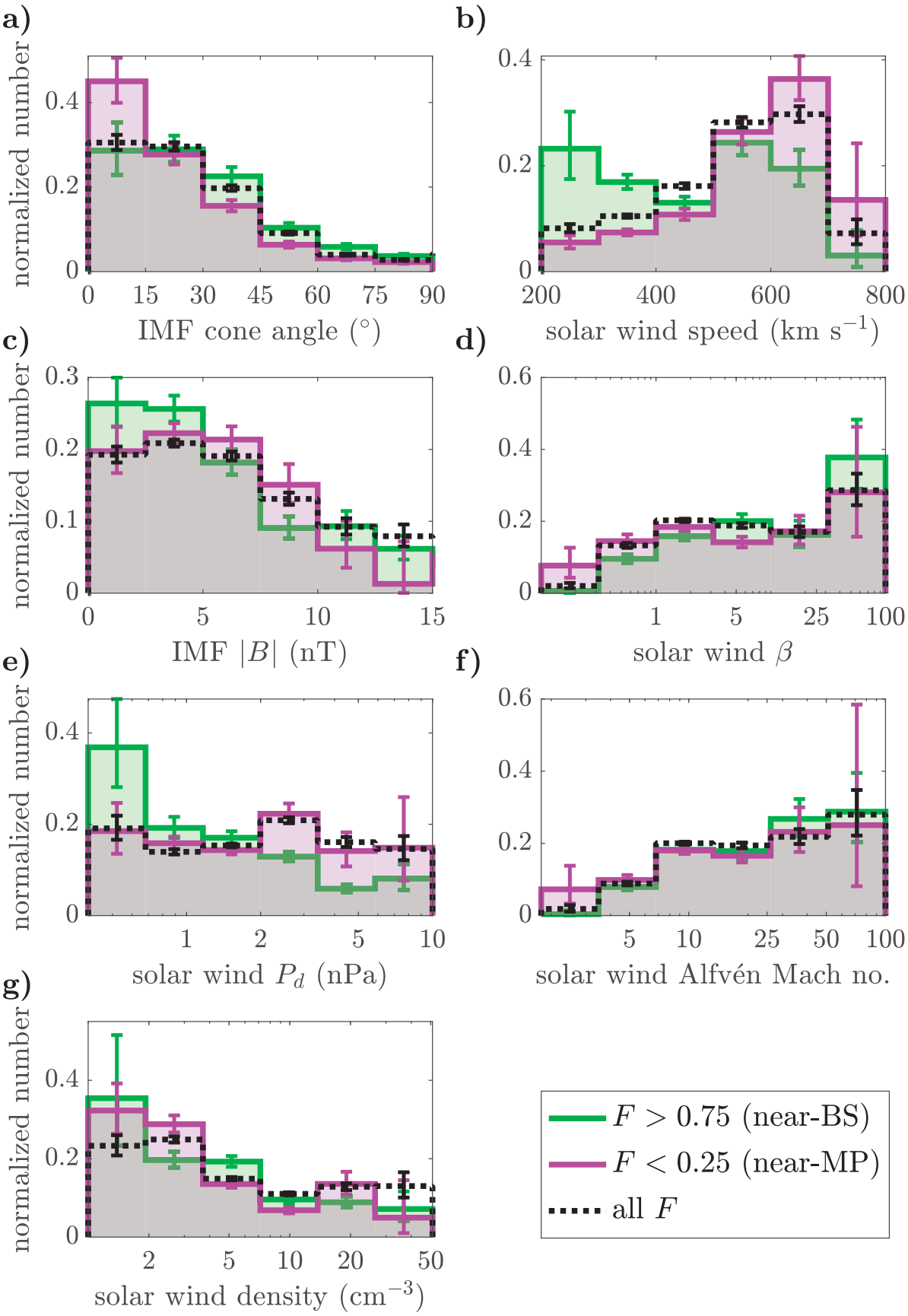

a)
b)
c)
d)
e)
f)
g)
normalized number
IMF cone angle (°)
solar wind speed (km s^{-1})
IMF $|B|$ (nT)
solar wind β
solar wind P_d (nPa)
solar wind Alfvén Mach no.
solar wind density (cm^{-3})
$F > 0.75$ (near-BS)
$F < 0.25$ (near-MP)
all F

Figure 5.

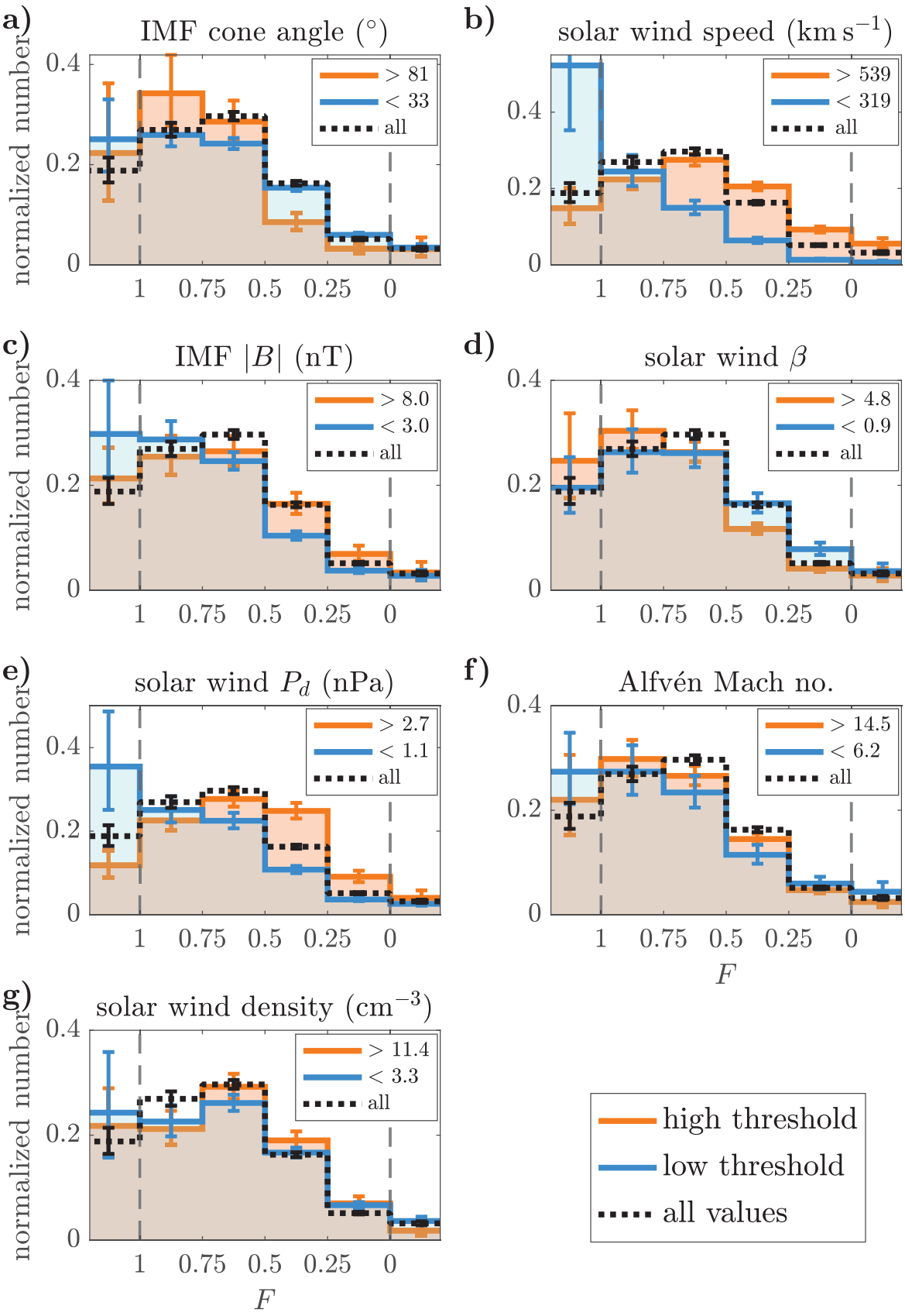
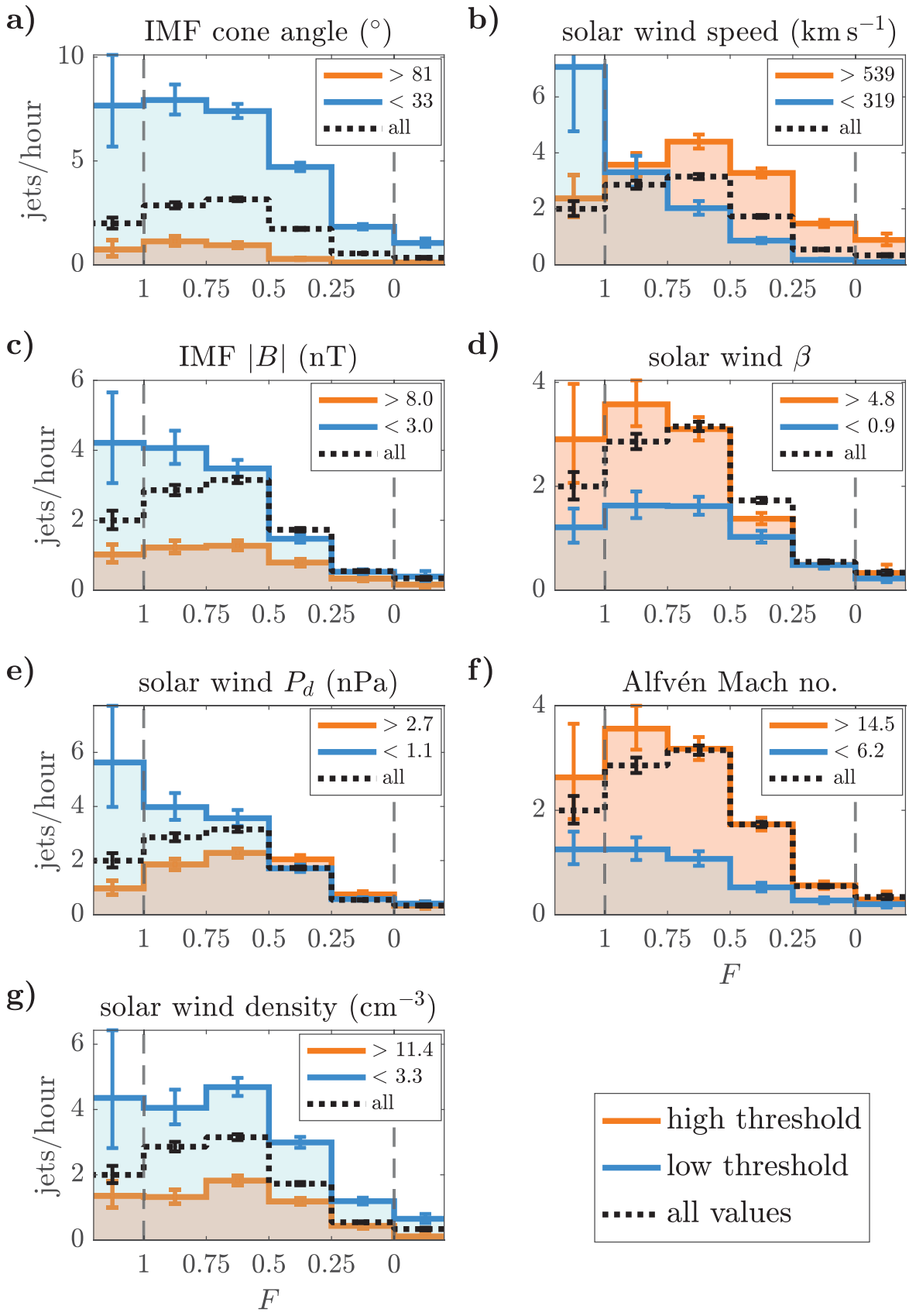

a)
IMF cone angle (°)
> 81
< 33
all
b)
solar wind speed (km s^{-1})
> 539
< 319
all
c)
IMF |B| (nT)
> 8.0
< 3.0
all
d)
solar wind β
> 4.8
< 0.9
all
e)
solar wind P_d (nPa)
> 2.7
< 1.1
all
f)
Alfvén Mach no.
> 14.5
< 6.2
all
g)
solar wind density (cm^{-3})
> 11.4
< 3.3
all
normalized number
0
0.2
0.4
1
0.75
0.5
0.25
0
F
high threshold
low threshold
all values

Figure 6.


a)
IMF cone angle (°)
jets/hour
> 81
< 33
all
b)
solar wind speed (km s^{-1})
> 539
< 319
all
c)
IMF |B| (nT)
> 8.0
< 3.0
all
d)
solar wind β
> 4.8
< 0.9
all
e)
solar wind P_d (nPa)
> 2.7
< 1.1
all
f)
Alfvén Mach no.
> 14.5
< 6.2
all
g)
solar wind density (cm^{-3})
> 11.4
< 3.3
all
1 0.75 0.5 0.25 0
F
high threshold
low threshold
all values